Original Article

MOLECULAR METABOLISM

The RhoGAP Stard13 controls insulin secretion through F-actin remodeling

Heike Naumann [1], **Thomas Rathjen** [2], **Matthew N. Poy** [2], **Francesca M. Spagnoli** [1,3,*]

ABSTRACT

Objective: Actin cytoskeleton remodeling is necessary for glucose-stimulated insulin secretion in pancreatic β-cells. A mechanistic understanding of actin dynamics in the islet is paramount to a better comprehension of β-cell dysfunction in diabetes. Here, we investigate the Rho GTPase regulator Stard13 and its role in F-actin cytoskeleton organization and islet function in adult mice.

Methods: We used Lifeact-EGFP transgenic animals to visualize actin cytoskeleton organization and dynamics *in vivo* in the mouse islets. Furthermore, we applied this model to study actin cytoskeleton and insulin secretion in mutant mice deleted for *Stard13* selectively in pancreatic cells. We isolated transgenic islets for 3D-imaging and perifusion studies to measure insulin secretion dynamics. In parallel, we performed histological and morphometric analyses of the pancreas and used *in vivo* approaches to study glucose metabolism in the mouse.

Results: In this study, we provide the first genetic evidence that *Stard13* regulates insulin secretion in response to glucose. Postnatally, *Stard13* expression became restricted to the mouse pancreatic islets. We showed that *Stard13* deletion results in a marked increase in actin polymerization in islet cells, which is accompanied by severe reduction of insulin secretion in perifusion experiments. Consistently, *Stard13*-deleted mice displayed impaired glucose tolerance and reduced glucose-stimulated insulin secretion.

Conclusions: Taken together, our results suggest a previously unappreciated role for the RhoGAP protein Stard13 in the interplay between actin cytoskeletal remodeling and insulin secretion.

Keywords F-actin; Insulin secretion; Islet; Pancreas; Lifeact; Stard13

1. INTRODUCTION

Pancreatic β-cells play a fundamental role in maintaining blood glucose homeostasis. Not only do they produce insulin but also they secrete the hormone in response to increases in blood glucose concentration [1,2]. Glucose-stimulated insulin secretion (GSIS) is the principal mechanism of insulin release by the β-cell [3–5]. This process coincides with actin cytoskeleton remodeling, during which glucose metabolites induce localized depolymerization of filamentous actin (F-actin) [3,6].

The actin cytoskeleton plays a complex role in regulating insulin release: it acts as a physical barrier, impeding the access of insulin granules to the cell periphery, but it also actively participates in it by providing a cytoskeletal track for insulin granule transport [4,6–10]. Yet, the molecular mechanisms responsible for F-actin remodeling in β-cells and their impact on insulin release are not clearly understood. Importantly, alterations in insulin secretion lead to type 2 diabetes [4,11]. Therefore, improving our understanding of how the cytoskeleton controls insulin secretion might shed new light on the pathophysiology of the disease as well as help to identify novel therapeutic strategies.

Actin cytoskeleton remodeling is regulated by the Rho-family of small GTPases in different cell types, including the pancreatic β-cells [12,13]. In mammals, the Rho-family of GTPases contains more than twenty members; Cdc42, Rac, and Rho are the best characterized members and most studied as regulators of actin assembly, each controlling the formation of filopodia, lamellipodia, and stress fibers, respectively [12,14]. Small GTPases cycle between a GTP-bound (active) and GDP-bound (inactive) conformation. This process is tightly regulated by distinct classes of proteins, including the guanine nucleotide exchange factors (GEFs), which mediate activation, the Rho GTPases-activating proteins (GAP), which lead to inactivation, and the guanine nucleotide dissociation inhibitors (GDI) [14,15]. Several studies have indicated Cdc42 and Rac1 GTPases as well as their effector protein PAK1, the GEF protein Tiam1, and RhoGDI as particularly important for glucose-stimulated insulin secretion *in vivo* and *in vitro* in mouse β-cells [6,13,16–19]. The Rho-ROCK pathway has also been implicated in β-cell function and insulin secretion [17,20,21]. For instance, pharmacological inhibition of Rho and ROCK leads to a significant increase in actin depolymerization and GSIS in rat primary β-cells and mouse insulinoma 6 (MIN6) cells [20,21]. However, the *in vivo* roles of Rho and Rho-dependent actin remodeling in insulin secretion remain to be assessed. To date, these investigations have been mostly hampered by the lack of suitable genetic models for studying actin remodeling and Rho signaling *in vivo* in β-cells. In particular, the reliable visualization of F-actin structures with sufficient

[1]Lab. of Molecular and Cellular Basis of Embryonic Development, Max-Delbrueck Center for Molecular Medicine, Robert-Roessle Strasse 10, Berlin 13125, Germany [2]Max-Delbrueck Center for Molecular Medicine, Robert-Roessle Strasse 10, Berlin 13125, Germany [3]Berlin Institute of Health (BIH), Berlin, Germany

*Corresponding author. E-mail: francesca.spagnoli@mdc-berlin.de (F.M. Spagnoli).

Received December 18, 2017 • Accepted December 24, 2017 • Available online 28 December 2017

https://doi.org/10.1016/j.molmet.2017.12.013

resolution and without interfering with cytoskeleton dynamics have represented a critical limitation to overcome.

To fill these gaps and gain insight into how actin cytoskeleton regulates insulin secretion, we used the Lifeact-EGFP transgenic mice to visualize F-actin in β-cells [22]. Further, we applied this model to study *in vivo* actin cytoskeleton and insulin secretion in mice deficient for the Rho GTPase regulator RhoGAP Stard13 that we previously identified in embryonic pancreas [23]. Postnatally, *Stard13* expression became restricted to the pancreatic islets. Here, we showed that *Stard13* deletion results in a marked increase in actin polymerization in islet cells, which is accompanied by severe reduction in insulin secretion in perifusion experiments. Consistently, animals displayed impaired glucose tolerance and reduced GSIS. Taken together, our results suggest a previously unappreciated role of the RhoGAP protein Stard13 as a key component of the insulin secretion machinery through actin cytoskeletal remodeling.

2. MATERIALS AND METHODS

2.1. Mouse strains, phenotypic characterization, and tissue preparation

The following mouse strains were used: Stard13flox$^{tm1.1FMS}$ mice [23], B6.FVB-Tg(Ipf1-cre)$^{1Tuv/Nci}$ [24], Tg(Ins2-cre)^{23Herr} [25], Tg(CAG-EGFP)$^{\#Rows}$ [22]. All animal experiments were performed in accordance with the rules and regulations of the LaGeso local authority. Efficiency of recombination in the *Pdx1-Cre* line was previously assessed in [23]. For the glucose tolerance test (GTT), mice were fastened overnight and blood was collected before and after intraperitoneal injection of glucose (2 g/kg body weight) at 15, 30, 60, and 120 min. Blood glucose levels were determined using a glucometer (Contour, Bayer). For glucose-stimulated insulin secretion (GSIS), fasted animals were injected intraperitoneally with glucose (2 g/kg body weight). Plasma insulin concentration was measured by an ultra-sensitive mouse insulin ELISA kit (Crystal Chem. Inc., Downers Grove, USA) at 0, 2, 5, 15 min time points after glucose injection. Plasma insulin concentration from random fed mice was determined by radioimmunoassay kit (Rat Insulin RIA #RI-13K, Merck-Millipore). For the measurement of insulin content, the pancreata were excised and weighted, and insulin was extracted by homogenization using a glass-Teflon homogenizer in acidic ethanol (2% concentrated HCl in 100% ethanol). After centrifugation, supernatants were collected, and the immunoreactive insulin in the supernatant was measured by radioimmunoassay kit (Rat Insulin RIA #RI-13K, Merck-Millipore).

2.2. Imaging analysis on isolated islets

For imaging analysis, islets were isolated from transgenic and non-transgenic control mice by collagenase digestion (640 U) at 37 °C for 15 min with mild shaking, as described previously [26]. Islets were picked by hand selection under a dissecting microscope, plated into channel slides (μ-slide VI 0.4, Ibidi, #80,606) and cultured overnight in RPMI 1640 medium supplemented with 10% FCS unless differently stated. Islets were stimulated afterwards with 8 or 16 mM glucose, where indicated. The next day, Z-stack acquisition of Lifeact-EGFP fluorescence was performed on a Zeiss LSM 700 confocal microscope. Subsequently, the islets were fixed for 30 min in 4% paraformaldehyde at RT and subjected to immunostaining analyses. Briefly, islets were permeabilized with 1% Triton X-100 in PBS for 20 min, blocked for 30 min in 10% donkey serum blocking solution and, subsequently, incubated with the indicated primary and secondary antibodies diluted in 1.5% donkey serum overnight at 4 °C. For latrunculin B treatment, islets were pre-incubated in the presence of 10 μM Latrunculin B or DMSO for 30 min and were then imaged. Images and time-lapse movies (45 s interval using a 63 × oil objective) were acquired on a Zeiss LSM 700; 3D projections and rendering were created using Zen 2010, Imaris 7.6.5 and ImageJ software.

2.3. Perifusion assays in isolated islets

Pancreatic islets were isolated from transgenic and non-transgenic control animals, as described above, and cultured overnight in RPMI 1640 medium supplemented with 10% FCS. We performed islet perifusion assays as previously described [27]. Briefly, 50 islets per condition were placed on a nylon filter in a plastic perifusion chamber and perifused with a modified KRBH buffer (137 mM NaCl, 2.7 mM KCl, 0.9 mM $CaCl_2$, 0.5 mM $MgCl_2$, 1.5 mM KH_2PO_4, 8.1 mM NaH_2PO_4, 20 mM Hepes pH 7.4, 0.2% BSA) containing various concentrations of glucose at a constant flow rate of 0.1 ml/min using the BioRep Perifusion System (Model No. PERI-4.2) maintained at 37 °C. Prior to fraction collection, the islets were primed for 30 min in a buffer containing 5.5 mM glucose and, subsequently, perifused with low-glucose (3.3 mM) for 8 min, followed by 15 min high-glucose (16.7 mM), 15 min low-glucose (3.3 mM) and a final step with 30 mM KCl + 3.3 mM glucose for 8 min.

Where indicated, islets were primed in the presence of 10 μM latrunculin B (Calbiochem #4,28,020) for 30 min and subsequently perifused with latrunculin B under low and high glucose stimulatory conditions as above. The fractions were collected every 1 min and insulin measured by radioimmunoassay (Rat Insulin RIA #RI-13K, Merck-Millipore).

2.4. Immunofluorescence and morphometric analyses

Mouse pancreata were fixed in 4% paraformaldehyde at 4 °C overnight. Subsequently, samples were equilibrated in 20% sucrose solution, embedded in Tissue-Tek OCT compound (Sakura, #4583) and cryosectioned at 10 μm-thickness. Immunofluorescence staining on cryosections was performed as previously reported [23]. Primary antibodies are listed in Supplementary Table 1. Image acquisition was done with a Zeiss LSM 700 confocal microscope. Briefly, for the morphometric analysis of the islets, the entire pancreas of 3 controls and 3 mutants per time-point was sectioned. Sections were stained for Insulin, Glucagon and Hoechst, imaged by tile-scan acquisition and evaluated at 100—300 μm interval for 6 M pancreata. Islet areas were measured using the AxioVision software (Zeiss). For the analysis of islet cellular composition, the insulin- and glucagon-specific areas were measured on confocal lsm files using the ROI tool in ImageJ. Fluorescence intensity was quantified in ImageJ software on split channels using the integrated density and corrected total cell fluorescence (CTCF) tools in individual cells or islets.

For z-stack analysis, individual islets in individual z-planes were defined as ROI, the fluorescence intensity within the ROIs was measured and the sum intensity values of multiple *z*-planes calculated. All results are expressed as mean ± s.e.m., and significance of differences between groups was evaluated with Student's t-test.

2.5. TEM

Pancreata from adult mice were fixed in phosphate-buffered 4% formaldehyde and post-fixed in 2% formaldehyde and 1% glutaraldehyde. After treatment with 1% OsO4, the samples were dehydrated and embedded in Poly/Bed 812 (Polysciences, Inc., Eppelheim, Germany). Ultrathin sections were stained with uranyl acetate and lead citrate and examined using a FEI Morgagni electron microscope. Digital images were taken with a Morada CCD camera and the iTEM software (Olympus Soft Imaging Solutions GmbH, Münster, Germany).

2.6. Statistical analyses

All results are expressed as mean ± standard deviation (s.d.) or standard error (s.e.m.), as indicated. Each experiment was repeated multiple times independently (at least ≥ 3). The significance of differences between groups was evaluated with Student's t-test or two-way ANOVA test, as appropriate. $p < 0.05$ was considered statistically significant.

3. RESULTS

3.1. Lifeact-EGFP labels F-actin in mouse pancreatic islets *in vivo*

Visualization of F-actin in living cells is critical for the study of cytoskeleton dynamics and actin-dependent cellular processes, such as cell migration, polarization, and regulated exocytosis [28]. Lifeact is a 17-amino-acid-long actin-binding peptide derived from yeast that specifically labels F-actin without affecting actin organization and dynamics [22]. The Lifeact-EGFP probe has been used previously to label individual cells in isolated mouse islets by adenoviral overexpression [29]. Here, to visualize the *in vivo* organization of actin cytoskeleton and F-actin dynamics in pancreatic islets, we used transgenic mice ubiquitously expressing the Lifeact peptide fused to EGFP, known as Lifeact-EGFP mice [22] (Figure 1). We isolated islets from adult pancreas of transgenic Lifeact-EGFP mice and characterized them by three-dimensional (3D) culturing and imaging (Figure 1). Native Lifeact-EGFP was directly acquired in living cells of islets cultured for 12 h in the presence of glucose (16 mM) (Figure 1B) as well as after fixation and whole-mount immunostaining (Figure 1C,D). In both conditions, we found that the actin cytoskeleton is labeled in all cells of the Lifeact-EGFP transgenic islets (Figure 1). Importantly, Lifeact-EGFP overlapped with Alexa Fluor™ 555-conjugated phalloidin staining, though the Lifeact-EGFP signal was brighter enabling visualization of F-actin in all types of specialized structures with a better signal-to-noise ratio compared to phalloidin (Figure 1C). To further characterize Lifeact-EGFP transgenic islets, we performed whole-mount immunostaining with antibodies against endocrine cell-specific markers, such as glucagon and insulin (Figure 1D). Lifeact-EGFP transgenic mouse islets displayed typical cellular composition and architecture, with glucagon cells at the periphery of the islet, forming a mantle-like structure, and insulin-positive cells in the core and representing the majority of the cells. In summary, islets isolated from Lifeact-EGFP mice are ideally suited for visualizing the actin cytoskeleton in islets and individual β-cells *in situ*.

3.2. Stard13 deficiency perturbs F-actin cytoskeleton organization in adult islets

Actin cytoskeleton dynamics is regulated by small GTPases of the Rho family [14,28], but how Rho signaling is locally controlled in pancreatic islets remains to be fully elucidated. Proteins of the RhoGAP family are

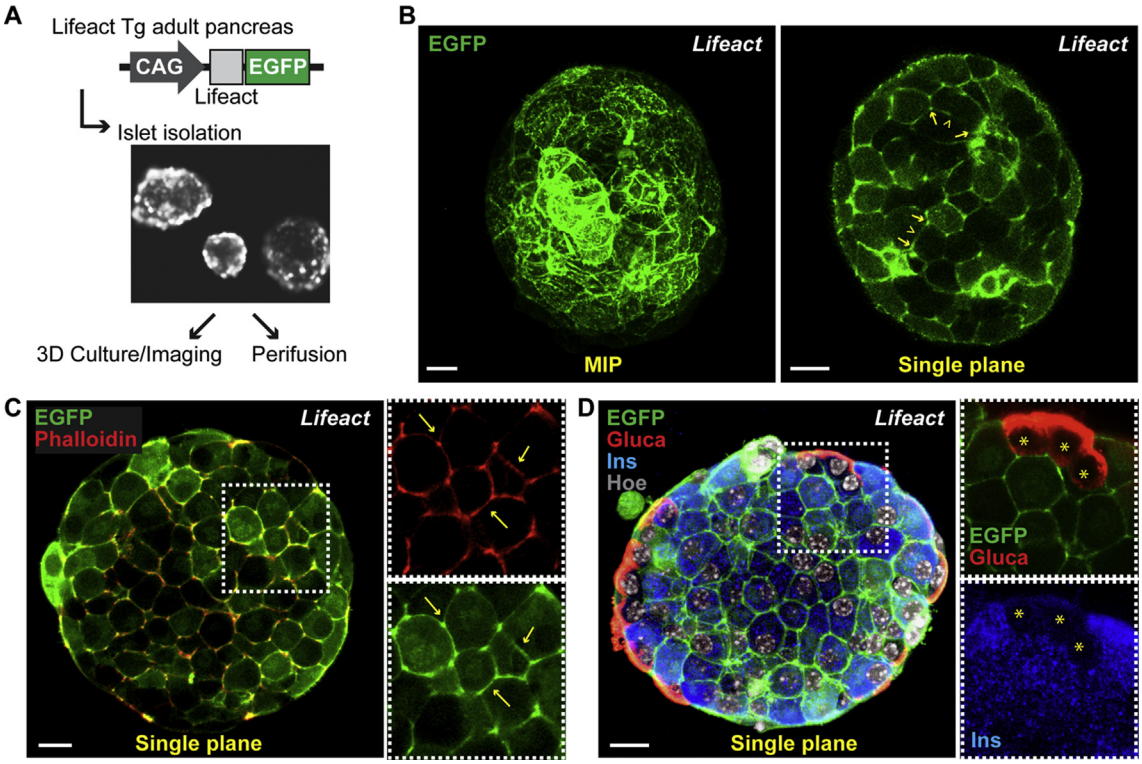

Figure 1: Characterization of the Lifeact-EGFP transgenic mouse islets. A) Schematic representation of the Lifeact-EGFP transgenic construct. Expression of the Lifeact peptide fused to EGFP is driven by CAG promoter [22]. Islets were isolated from Lifeact-EGFP adult mice and cultured either for 3D imaging or perifusion assays. **B**) Imaging of native Lifeact-EGFP (green) in live pancreatic islets. On the left, representative maximum intensity projection (MIP) of consecutive optical sections of a pancreatic mouse islet cultured for 12 h in the presence of glucose (16 mM); on the right, a single optical section (Single plane). Lifeact-EGFP signal labels all islet cells with a distribution more pronounced at the cellular edges (arrows) than along the cell faces (arrowheads). This is consistent with the labeling distribution observed in individual β-cells upon Lifeact-EGFP adenoviral infection of isolated mouse islets [29]. **C**) Representative single plane confocal image of whole-mount immunofluorescence staining of Lifeact-EGFP transgenic mouse islets for Phalloidin in red and Lifeact-EGFP in green. Insets show split channels (green and red) of boxed area; arrows indicate overlapping stainings. **D**) Representative single plane confocal image of whole-mount immunofluorescence of Lifeact-EGFP transgenic mouse islets for glucagon (Gluca, red) and insulin (Ins, blue), in green Lifeact-EGFP. Hoechst 33342 was used as nuclear counterstain. Insets show split channels of boxed area at higher magnification; stars indicate glucagon-positive cells which are negative for insulin. Bar, 10 um.

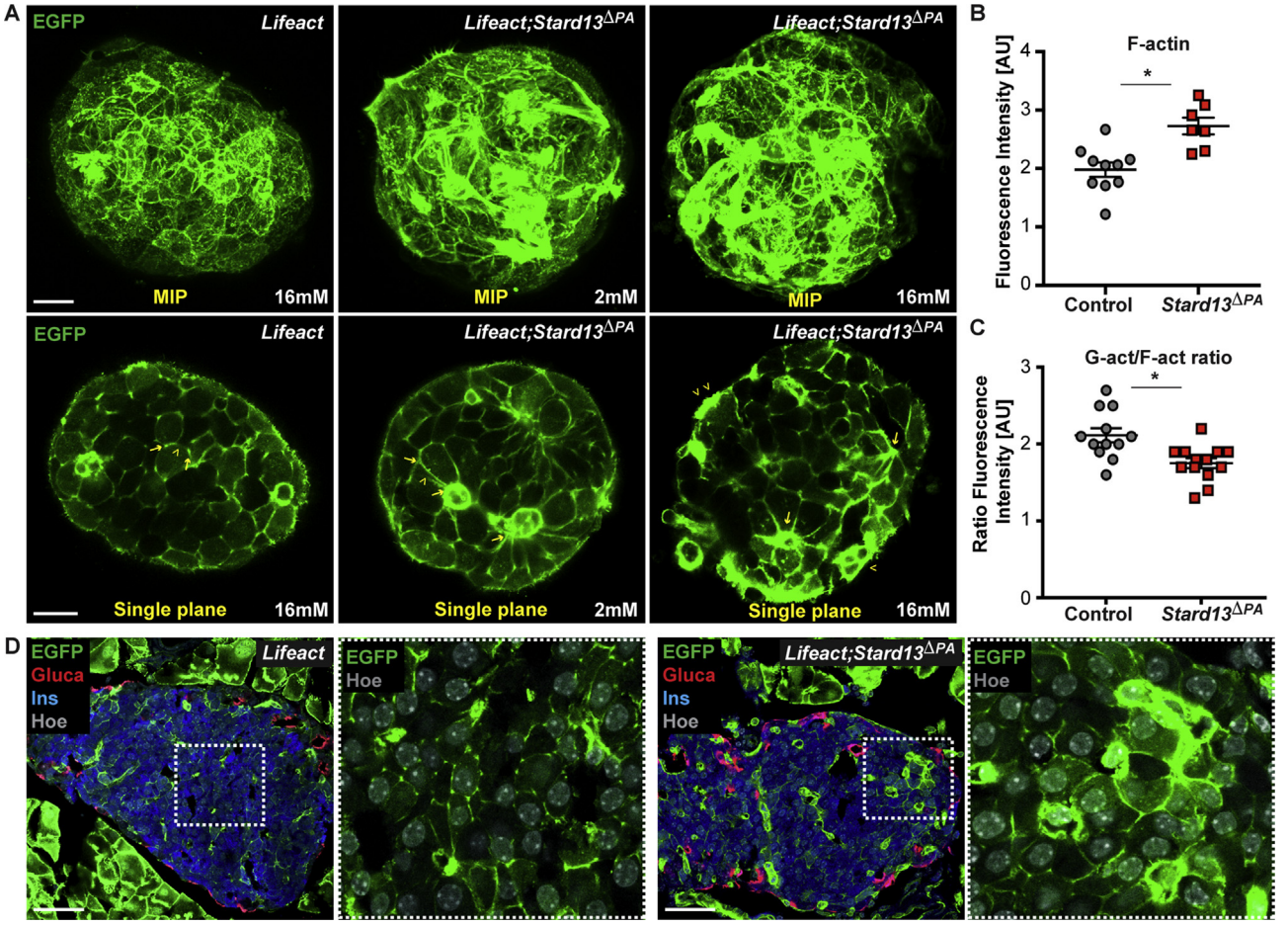

Figure 2: Disorganization of F-actin cytoskeleton in the absence of *Stard13* in pancreatic islets. A) Imaging of native Lifeact-EGFP (green) in *Lifeact* control and *Lifeact;Stard13*$^{\Delta PA}$ pancreatic islets. Representative MIPs and single optical sections of islets cultured for 12 h in the presence of low (2 mM) and high glucose (16 mM). Arrowheads indicate staining along the cell membranes; arrows indicate cellular edges. Bar, 20 um. **B**) Dot plot quantification of Lifeact fluorescence intensity in control and *Stard13*$^{\Delta PA}$ islets. ($n = 10$ islets from three independent pancreatic samples per genotype) *$p < 0.05$. **C**) Ratio of G-actin and F-actin fluorescence intensity in control and *Stard13*$^{\Delta PA}$ islets. Adult pancreatic tissue sections were stained with Phalloidin-Alexa Fluor™ 555 and Deoxyribonuclease I-Alexa Fluor™ 488 for the simultaneous detection of filamentous actin (F-actin) and unpolymerized actin (G-actin), respectively (Supplementary Fig. 2). Quantification was performed on at least 12 islets, 5 cells per islet, from three independent pancreatic samples per genotype. *$p < 0.05$ **D)** Immunofluorescence analysis on cryosections of adult pancreatic tissues from *Lifeact* control and *Lifeact;Stard13*$^{\Delta PA}$ transgenic animals. Glucagon (Gluca, red), insulin (Ins, blue), in green Lifeact-EGFP and Hoechst 33342 was used as nuclear counterstain. Insets show EGFP and Hoechst channels of boxed area at higher magnification. Bar, 50 um.

prime candidates for such activity [14,15]. We previously identified a Rho-GTPase regulator, the RhoGAP Stard13, for being expressed in the pancreas throughout embryonic development and required for F-actin cytoskeleton remodeling in pancreatic progenitors [23]. Interestingly, shortly before birth *Stard13* expression became restricted to the endocrine islets (Supplementary Fig. 1). To investigate whether *Stard13* plays a role in the organization of the actin cytoskeleton in adult islets, we generated a pancreas-specific deletion of *Stard13* using *Pdx1-Cre* (*Stard13*$^{flox/flox}$*;Pdx1-Cre*; hereafter referred to as *Stard13*$^{\Delta PA}$), as previously reported [23]. Next, to visualize F-actin organization, we intercrossed the *Stard13*$^{\Delta PA}$ and Lifeact-EGFP transgenic mice (hereafter referred to as *Lifeact;Stard13*$^{\Delta PA}$). Pdx1-Cre negative littermates served as negative controls. To perform 3D imaging of intact islets, we isolated pancreatic islets from *Lifeact;Stard13*$^{\Delta PA}$ and control animals and examined native Lifeact-EGFP in living cells (Figure 2A). Importantly, we found marked differences in F-actin cytoskeleton organization between control and *Stard13*$^{\Delta PA}$ islet cells: control cells displayed a thin cortical actin network and fine-mesh structures, while in mutant cells the meshwork's density was increased and bundles of actin fibers were visible beneath the cell membrane (Figure 2A). The increase in F-actin density was also reflected in the higher levels of Lifeact-EGFP fluorescence intensity in mutant islets compared to controls; by contrast, no differences were measured in insulin staining and distribution of membrane markers, including E-cadherin and GLUT2, which displayed a normal edge and vertex organization [29,30] (Figure 2B, Supplementary Figs. 2A–C). A similar abnormal cytoskeleton arrangement was also detectable on fixed adult pancreatic tissues of *Stard13*$^{\Delta PA}$ animals, which displayed an accumulation of F-actin in islets embedded in their native environment (Figure 2D). To further characterize the cytoskeleton changes observed in the absence of *Stard13*, we used fluorescent probes for simultaneous detection of monomeric globular actin (G-actin) and filamentous actin (F-actin) in pancreatic islets [12,14] (Supplementary Fig. 2D). In line with F-actin accumulation, we found that the ratio between G-actin and F-actin is decreased in mutant islets as compared to controls (Figure 2C).

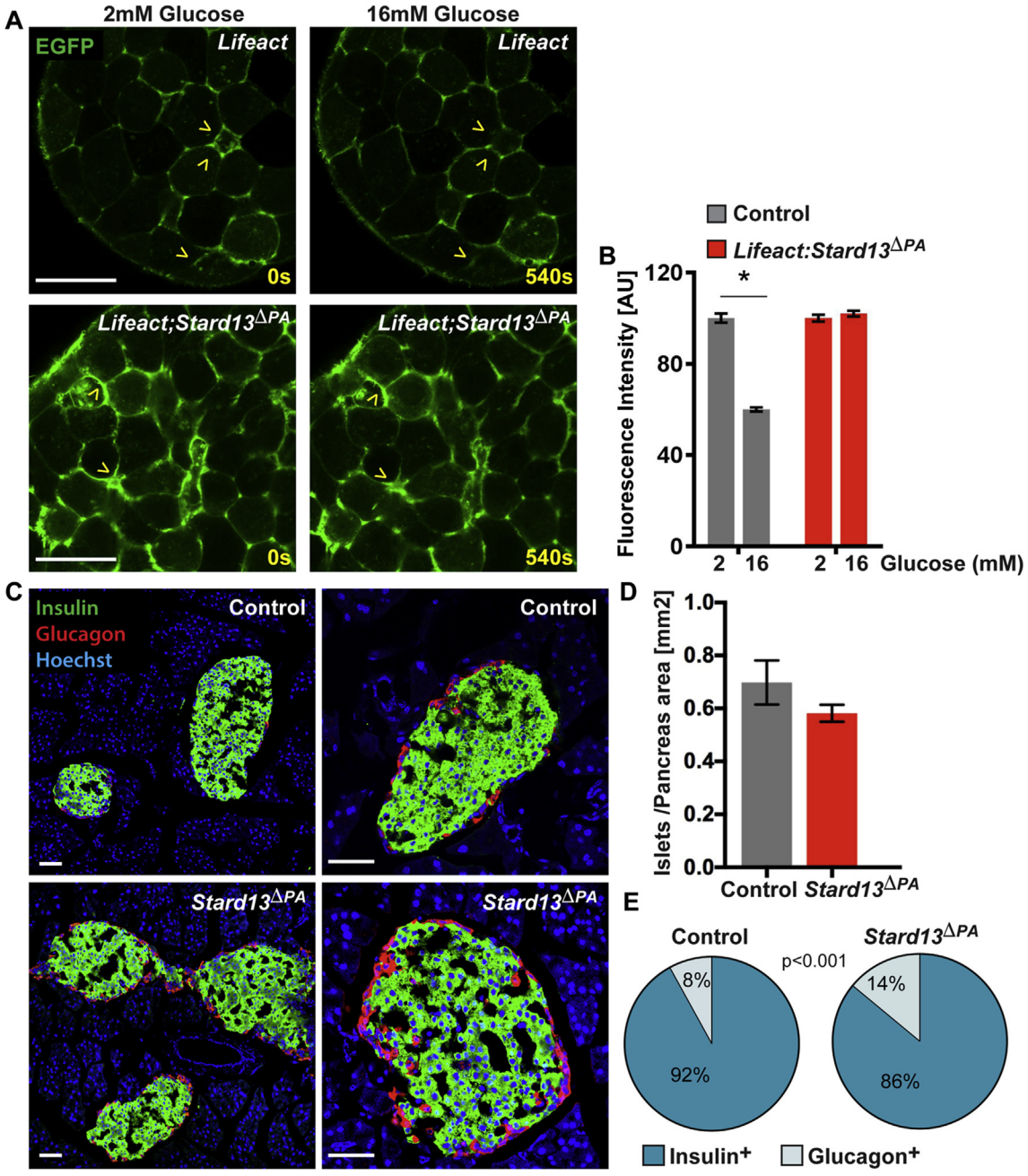

Figure 3: *Stard13* is required for F-actin cytoskeleton remodeling in islets upon glucose stimulation. **A**) Representative still image frames from time-lapse experiments of *Lifeact* control and *Lifeact;Stard13*$^{\Delta PA}$ living pancreatic islets cultured in the presence of low glucose (2 mM) and then stimulated with high glucose (16 mM). Arrowheads indicate native Lifeact-EGFP (green) along the cell membranes. Actin remodeling upon addition of glucose is visible in control islets but not in the mutants. Bar, 20 um. **B**) Quantification of Lifeact fluorescence intensity in control and *Lifeact;Stard13*$^{\Delta PA}$ islets cultured with low (2 mM) and high glucose (16 mM). (n = 10 islets). *p < 0.05. **C)** Immunofluorescence analysis of insulin (green) and glucagon (red) on control and *Stard13*$^{\Delta PA}$ adult pancreatic tissues. Hoechst (blue) was used as nuclear counterstain. Bar, 50 um. **D)** Morphometric analysis of islet surface area in control and *Stard13*$^{\Delta PA}$ pancreata at 6 months. Islet sectional area was normalized *versus* the total pancreas area. (n = 5). **E)** Portion of insulin and glucagon area *versus* total area in adult control and *Stard13*$^{\Delta PA}$ mouse islets. (n = 10 mice). p < 0.001.

3.3. Stard13 is required for actin remodeling in β-cells during GSIS

Glucose stimulation rapidly promotes F-actin remodeling to mobilize insulin granules to the cell periphery, which is a requisite for proper GSIS from the β-cells [6]. Notably, time-lapse imaging of whole islets showed that the F-actin network remained intact in *Lifeact;Stard13*$^{\Delta PA}$ islets and its abnormal distribution did not change in response to increasing concentration of glucose, which instead occurred in control islets (Figure 3A,B). These results suggest that *Stard13* activity is required for actin remodeling in β-cells in response to glucose stimulation.

Next, we asked whether the F-actin accumulation and disorganization observed in *Stard13*$^{\Delta PA}$ islets affect insulin secretion dynamics. To this aim, we performed islet perifusion studies (Figure 4A). Islets were isolated from control and *Stard13*$^{\Delta PA}$ adult mouse pancreas and challenged with increasing concentration of glucose. At low levels of

glucose (3.3 mM), insulin secretion did not measurably differ between mutant and control islets. By contrast, in high glucose conditions (16.7 mM), islets from *Stard13*$^{\Delta PA}$ mice exhibited a significant reduction in insulin release compared to control islets during both first and second-phase secretion (Figure 4A). Islets from *Stard13*$^{\Delta PA}$ mice had blunted insulin secretion in response to KCl-stimulation too, which is compatible with a disrupted F-actin network [10,31] (Figure 4A).

Accordingly, we previously reported that *Stard13*$^{\Delta PA}$ mice displayed impaired glucose tolerance at three months after birth when compared to control animals of the same age [23]; this defect became more pronounced with aging (Supplementary Fig. 3). The basal plasma insulin levels did not differ between mutant and control animals (Figure 4C), while the increase in plasma insulin in response to glucose injection was blunted in *Stard13*$^{\Delta PA}$ mice when compared to controls (Figure 4D). Together, the *in vivo* GSIS and the reduced ability of *Stard13*$^{\Delta PA}$ mice to clear blood glucose in the GTT experiment are consistent with the islet perifusion results, suggesting a function of *Stard13* in β-cells to control insulin secretion by regulating actin dynamics.

Decreased insulin secretion could also reflect changes in β-cell mass, differentiation state, and/or defects in insulin production or granule biogenesis [32–34]. To distinguish among these possibilities, we first examined the endocrine islet area and pancreatic insulin content, which were both comparable between age-matched control and *Stard13*$^{\Delta PA}$ mice (Figures 3C,D, 4B). The architecture of *Stard13*$^{\Delta PA}$ islets overall resembled that of control islets, displaying the typical presence of β-cells within the islet core and α-cells at the periphery (Figure 3C). Quantification of cellular composition revealed a slight but significant increase (~6%) in α-cells *versus* β-cell area in *Stard13*-deficient mice compared with controls (Figure 3E). Nevertheless, this is unlikely to account for the reduced insulin secretion seen in the perifusion experiment.

To determine whether insulin secretory vesicle formation was impaired in the absence of *Stard13*, we employed transmitted electron

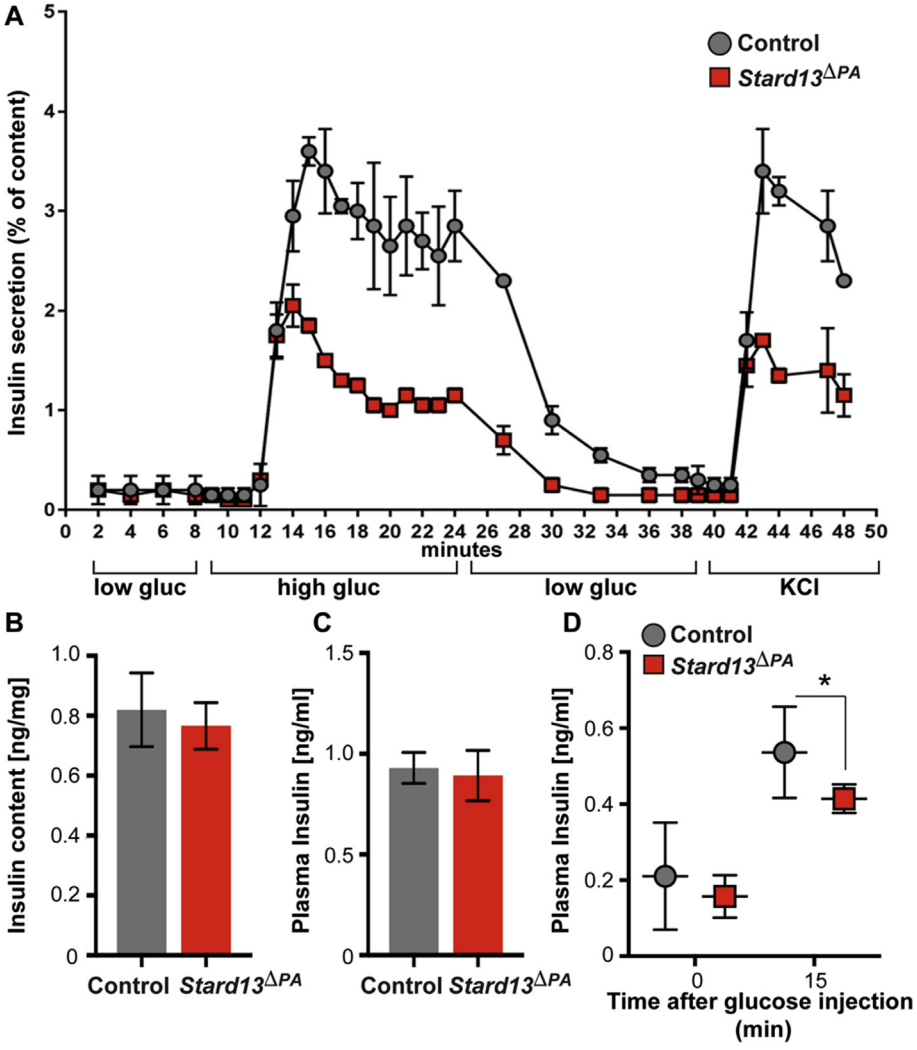

Figure 4: Insulin secretion is reduced in Stard13-deficient mouse models. A) Dynamics of GSIS by islet perifusion from control and *Stard13*$^{\Delta PA}$ mouse pancreas. Islets incubated in KRBH buffer containing 3.3 mM glucose (low) were stimulated with 16.7 mM glucose (high), returned to low conditions, and finally, perifused with 30 mM KCl, as indicated. Insulin release kinetics showed biphasic responsiveness from islets isolated from control mice that mimicked those previously reported [39]. Insulin values in collected fractions are presented as secreted insulin normalized to islet insulin content (n = 3 animals per genotype). ANOVA test, $p < 0.001$. **B)** Pancreas insulin content and **C)** plasma insulin in the random-fed condition is similar between control and *Stard13*$^{\Delta PA}$ mice (n = 6). **D)** Plasma insulin after intraperitoneal injection of glucose (2 g/kg body weight) is lower in *Stard13*$^{\Delta PA}$ mice compared to control animals. (n = 7) *$p < 0.05$.

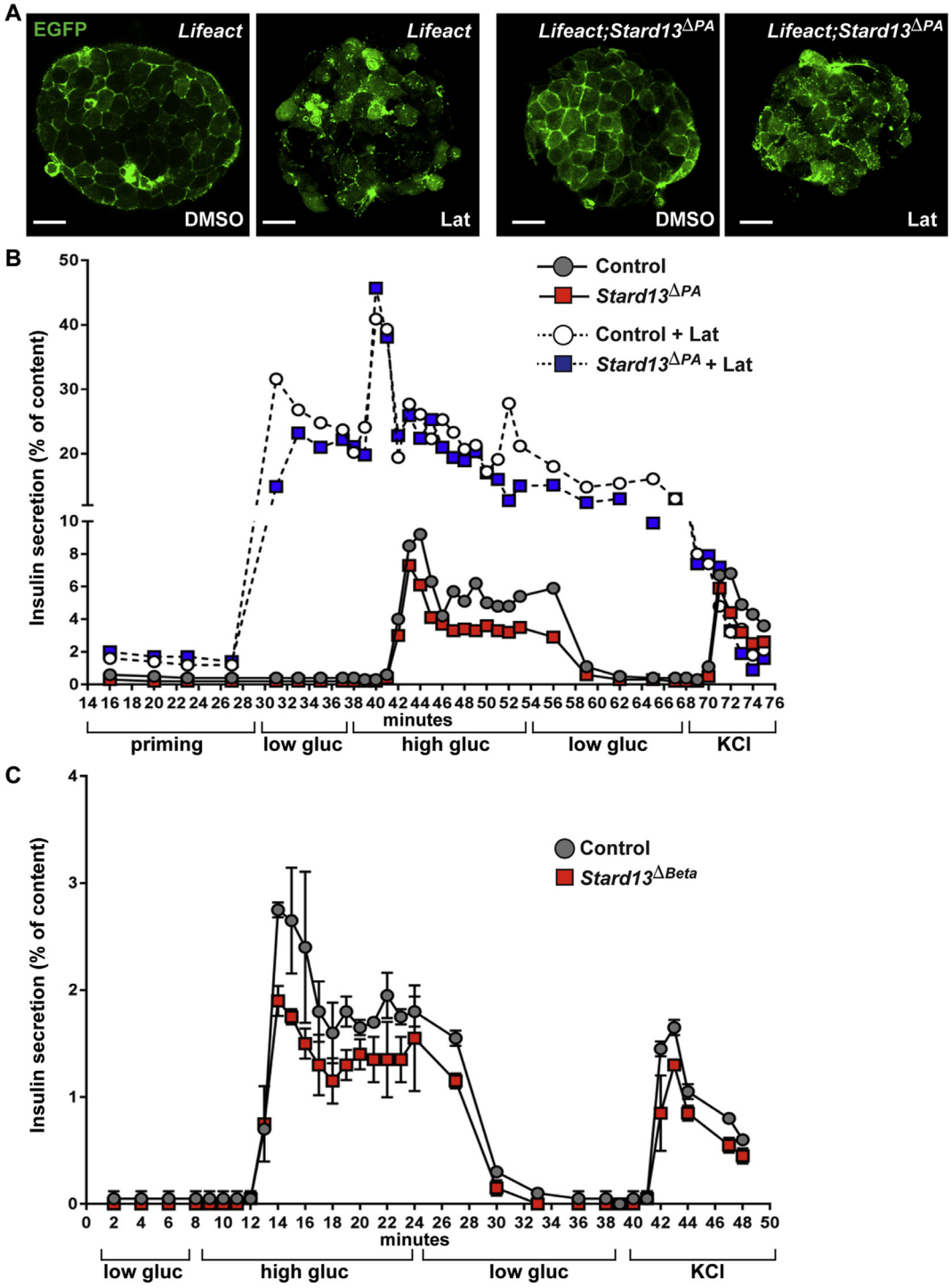

Figure 5: Insulin secretion is restored in *Stard13*-deficient islets upon treatment with latrunculin. A) Representative single plane confocal images of *Lifeact* control and *Lifeact;Stard13*$^{\Delta PA}$ pancreatic islets cultured for 30 min in KRBH buffer (supplemented with 5.5 mM Glucose) in the presence of DMSO or 10 μM Latrunculin B (Lat). Bar, 20 μm. **B)** Representative islet perifusion assay from control and *Stard13*$^{\Delta PA}$ mouse pancreas either left untreated or treated with 10 μM Latrunculin B during the entire duration of the perifusion assay. Isolated islets were first incubated in KRBH buffer containing 5.5 mM glucose (priming) for 30 min; next, the islets were first exposed to 3.3 mM glucose (low), stimulated with 16.7 mM glucose (high), returned to low conditions, and, finally, perifused with 30 mM KCl, as indicated. Insulin values in collected fractions are presented as secreted insulin normalized to islet insulin content. (n = 3). **C)** GSIS assay by islet perifusion from control and *Stard13*$^{\Delta Beta}$ mice. Insulin content in collected fractions is presented as secreted insulin normalized to islet insulin content percentage of insulin secreted (n = 3). ANOVA test, $p < 0.001$.

microscopy (TEM). Ultrastructural examination of β-cells from control and *Stard13*$^{\Delta PA}$ islets revealed the presence of mature and immature insulin granules in a similar proportion (Supplementary Figs. 3E,F), ruling out impaired insulin granule biogenesis. Taken together, these findings suggest that insulin production and storage are not significantly affected in the mutant pancreas, but the observed defects in insulin secretion arise from impaired F-actin remodeling.

To directly address whether actin organization is responsible for the insulin secretion defects, we treated the *Stard13*$^{\Delta PA}$ islets with the actin depolymerization agent latrunculin B and, subsequently, performed islet perifusion studies (Figure 5). As expected, latrunculin B treatment rapidly abolished cortical actin staining in islets, consistent with previous reports [10,20,36]. Specifically, we found that cortical F-actin becomes fragmented into small clusters scattered throughout the cells of both control and *Lifeact;Stard13*$^{\Delta PA}$ islets (Figure 5A). Moreover, exposure to latrunculin B markedly potentiated GSIS when compared with untreated islets from both control and mutant *Stard13*$^{\Delta PA}$ mice (Figure 5B). These results indicate that insulin secretion is rescued when actin is depolymerized in mutant islets, further supporting a role for Stard13 in F-actin cytoskeleton remodeling in the β-cell.

3.4. Stard13 is required for insulin secretion in β-cells

Finally, to determine the function of *Stard13* specifically in β-cells, we generated *Stard13*$^{flox/flox}$*;RIP-Cre* [25] (hereafter referred to as *Stard13*$^{\Delta Beta}$) mice. Deletion of *Stard13* in differentiating β-cells did not affect pancreas formation and organ weight (Supplementary Fig. 3), which is different from the early phenotype associated with the *Stard13*$^{\Delta PA}$ pancreata [23]. Nevertheless, *Stard13* deficiency in β-cells had a direct impact on insulin release from isolated perifused mouse islets (Figure 5C). Specifically, we found a reduction of insulin secretion in response to glucose in *Stard13*$^{\Delta Beta}$ perifused islets as compared to control adult islets, whereas total insulin content in the isolated islets and insulin plasma levels in fed state were unchanged (Supplementary Fig. S3 and data not shown). Note that differences in the insulin secretion response of control islets were visible during the perifusion experiments (Figures 4A, 5B,C) To avoid these variations, that are possibly due to islet preparation, we always isolated and simultaneously tested both control and mutant islets for each perifusion assay shown in this study.

Together, these results revealed that GSIS is impaired when *Stard13* is deficient in β-cells and are consistent with the impaired glucose-responsive insulin secretion observed in *Stard13*$^{\Delta PA}$ islets.

4. DISCUSSION

In this study, we have uncovered the essential role of the RhoGAP Stard13 in ensuring insulin secretion in response to glucose. Interestingly, Stard13 played a prominent role in both acute and secondary phases of GSIS, with no effect on insulin granule biogenesis, insulin content and β-cell morphology. Deletion of *Stard13* destabilized the β-cell cytoskeleton, leading to a thicker and disorganized F-actin network, and hampered its remodeling in response to glucose. Importantly, latrunculin B-dependent depolymerization of F-actin restores insulin secretion in islets from *Stard13*-deficient pancreas. Taken together, these results suggest that F-actin cytoskeleton remodeling is under the local control of the RhoGAP Stard13 in the β-cell.

The continuous turnover of cortical actin filaments enables animal cells to quickly respond to external stimuli and readily adapt to mechanical cues or biochemical signaling [28]. A prime example of this is represented by the GSIS in pancreatic β-cells, wherein glucose stimulation rapidly promotes F-actin remodeling to mobilize insulin granules to the cell periphery [6]. Consistently, treatment with the actin depolymerizing agent latrunculin B has been demonstrated to potentiate GSIS [10]. Additionally, F-actin-associated proteins, such as MLCK, myosin IIA, and FAK, have been implicated in insulin release [6,8,35–37]. Our study indicates Stard13 as a novel regulator of actin organization and function in β-cells that may occur through both direct and indirect mechanisms. We previously reported that Stard13 regulates Rho signaling during pancreas development [23]. In the absence of *Stard13*, uninhibited Rho activity hampered actin cytoskeleton remodeling, leading to F-actin fibers accumulation in mouse pancreatic progenitor cells [23]. Here, our results suggest a functionally conserved role for this RhoGAP protein in adult islets, underlying cortical F-actin depolymerization during insulin secretion from β-cells. The impact of Stard13 deficiency is indeed measurable only upon glucose challenge, but not in low-glucose conditions. This is also supported by the glucose intolerance phenotype observed in *Stard13*$^{\Delta PA}$ mice and it can explain the absence of an overt diabetic phenotype in these mutant animals.

Focal adhesion actin-remodeling events also contribute to insulin secretion [6,36]. Both genetic inactivation and pharmacological inhibition of FAK have suggested its indirect regulation of F-actin remodeling and insulin secretion [35,36]. Importantly, Stard13 has been shown to localize to focal adhesions and, in certain contexts, to spatially regulate RhoA activation at these specialized structures [38]. It is therefore possible that Stard13 might regulate GSIS through focal adhesion actin-remodeling events and not only through cortical actin remodeling. Finally, crosstalk between different Rho GTPases family members is known to regulate various cellular processes and might be at play in insulin secretion too [14]. Further investigation is required to address whether in the absence of Stard13 the uninhibited Rho activity might indirectly affect Cdc42 or Rac1, which are well-recognized regulators of the second-phase insulin secretion [6,13,39].

The mechanisms that regulate actin cytoskeleton dynamics (*e.g.* assembly and disassembly) *in vivo* are poorly understood, largely because of the difficulty to visualize filamentous F-actin structures. Lifeact is widely used for F-actin visualization in cells and tissues without significantly interfering with actin dynamics *in vitro* or *in vivo* [22,40]. Here, we found a strong expression of the Lifeact-EGFP transgene *in vivo* in β-cells and a clear labeling of the actin cytoskeleton. Thus, Lifeact-EGFP transgenic animals are likely to be a useful tool for further elucidating the role of actin in trafficking and exocytosis of insulin secretory granules as well as the mechanisms underlying actin regulation in the β-cells. For instance, such *in vivo* model will enable to address in details the mechanisms underlying Stard13-mediated insulin secretion function by characterizing the actin microtubule-mediated transport of the granules over time as well as their relationship with focal adhesions [9,35,36,41].

Alterations in insulin secretion are among the causes of diabetes [11]. Our data support a specific role of Stard13-mediated actin remodeling in the regulation of GSIS in β-cells and highlight its potential relevance to the pathogenesis of type 2 diabetes. In line with this, the Rho-ROCK pathway has been previously implicated in diabetes [8,20,42]. For example, the expression of RhoA has been reported to be increased in pancreatic islets of diabetic mouse models [20,21]. Furthermore, human islets of patients with type 2 diabetes exhibit a strong decrease in PAK1, a downstream effector of Cdc42 and Rac1 signaling [16]. Collectively, these findings highlight the importance of the Rho-actin cytoskeleton in β-cell function and might have important

implications for the understanding of β-cell dysfunction in type 2 diabetes and the development of possible therapeutic targets for the disease.

AUTHOR CONTRIBUTIONS

F.M.S. conceived and directed the study. H.N. performed all the experiments and analyzed the data together with FMS. T.R. and M.P. assisted with islet isolation and perifusion experiments. F.M.S. wrote the manuscript and generated figures. All authors proofread and approved the final manuscript.

ACKNOWLEDGEMENTS

We thank all members of the Spagnoli lab. for helpful discussion, Christin Zasada for help with R-code and Christina Eichhorn for statistical analysis. This work was supported by funds from the Helmholtz Association, The F.M.S. lab. is supported by the ERC-POC grant (TheLiRep #641036), GIF (I-1308-203), BIH (Tr. PhD grant #42200001) and EFSD/AZ grants. The authors declare that they have no competing financial interests. The C57BL/6 Lifeact-EGFP mice were kindly provided by Dr. Roland Wedlich-Soeldner and the RIP-Cre mice by Dr. Pedro Herrera.

CONFLICT OF INTEREST

None declared.

APPENDIX A. SUPPLEMENTARY DATA

Supplementary data related to this article can be found at https://doi.org/10.1016/j.molmet.2017.12.013.

REFERENCES

[1] Cerasi, E., Luft, R., 1967. The plasma insulin response to glucose infusion in healthy subjects and in diabetes mellitus. Acta Endocrinologica 55:278—304.
[2] Boland, B.B., Rhodes, C.J., Grimsby, J.S., 2017. The dynamic plasticity of insulin production in beta-cells. Molecular Metabolism 6:958—973.
[3] Rorsman, P., Renström, E., 2003. Insulin granule dynamics in pancreatic beta cells. Diabetologia 46:1029—1045.
[4] Seino, S., Shibasaki, T., Minami, K., 2011. Dynamics of insulin secretion and the clinical implications for obesity and diabetes. Journal of Clinical Investigation 121:2118—2125.
[5] MacDonald, P., 2011. Signal integration at the level of ion channel and exocytotic function in pancreatic β-cells. American Journal of Physiology — Endocrinology and Metabolism 301:E1065—E1069.
[6] Kalwat, M.A., Thurmond, D.C., 2013. Signaling mechanisms of glucose-induced F-actin remodeling in pancreatic islet beta cells. Experimental & Molecular Medicine 45:e37.
[7] Orci, L., Gabbay, K., Malaisse, W., 1972. Pancreatic beta-cell web: its possible role in insulin secretion. Science 175:1128—1130.
[8] Arous, C., Halban, P.A., 2015. The skeleton in the closet: actin cytoskeletal remodeling in beta-cell function. American Journal of Physiology — Endocrinology and Metabolism 309:E611—E620.
[9] Hoboth, P., Müller, A., Ivanova, A., Mziaut, H., Dehghany, J., Sönmez, A., et al., 2015. Aged insulin granules display reduced microtubule-dependent mobility and are disposed within actin-positive multigranular bodies. Proceedings of the National Academy of Sciences U S A 112:E667—E676.
[10] Thurmond, D., Gonelle-Gispert, C., Furukawa, M., Halban, P., Pessin, J., 2003. Glucose-stimulated insulin secretion is coupled to the interaction of actin with the t-SNARE (target membrane soluble N-ethylmaleimide-sensitive factor attachment protein receptor protein) complex. Molecular Endocrinology 17:732—742.
[11] Ashcroft, F., Rorsman, P., 2012. Diabetes mellitus and the β cell: the last ten years. Cell 148:1160—1171.
[12] Etienne-Manneville, S., Hall, A., 2002. Rho GTPases in cell biology. Nature 420:629—635.
[13] Wang, Z., Thurmond, D.C., 2009. Mechanisms of biphasic insulin-granule exocytosis - roles of the cytoskeleton, small GTPases and SNARE proteins. Journal of Cell Science 122:893—903.
[14] Hodge, R., Ridley, A., 2016. Regulating Rho GTPases and their regulators. Nature Reviews Molecular Cell Biology 17:496—510.
[15] Tcherkezian, J., Lamarche-Vane, N., 2007. Current knowledge of the large RhoGAP family of proteins. Biology of the Cell 99:67—86.
[16] Wang, Y., Oh, E., Clapp, D., Chernoff, J., Thurmond, D., 2011. Inhibition or ablation of p21-activated kinase (PAK1) disrupts glucose homeostatic mechanisms in vivo. Journal of Biological Chemistry 286:41359—41367.
[17] Kowluru, A., 2010. Small G proteins in islet beta-cell function. Endocrine Reviews 31:52—78.
[18] Nevins, A., Thurmond, D., 2003. Glucose regulates the cortical actin network through modulation of Cdc42 cycling to stimulate insulin secretion. American Journal of Physiology — Cell Physiology 285:C698—C710.
[19] Asahara, S., Shibutani, Y., Teruyama, K., Inoue, H., Kawada, Y., Etoh, H., et al., 2013. Ras-related C3 botulinum toxin substrate 1 (RAC1) regulates glucose-stimulated insulin secretion via modulation of F-actin. Diabetologia 56:1088—1097.
[20] Hammar, E., Tomas, A., Bosco, D., Halban, P., 2009. Role of the Rho-ROCK (Rho-Associated kinase) signaling pathway in the regulation of pancreatic beta-cell function. Endocrinology 150:2072—2079.
[21] Liu, X., Yan, F., Yao, H., Chang, M., Qin, J., Li, Y., et al., 2014. Involvement of RhoA/ROCK in insulin secretion of pancreatic β-cells in 3D culture. Cell and Tissue Research 358:359—369.
[22] Riedl, J., Flynn, K.C., Raducanu, A., Gartner, F., Beck, G., Bosl, M., et al., 2010. Lifeact mice for studying F-actin dynamics. Nature Methods 7:168—169.
[23] Petzold, K.M., Naumann, H., Spagnoli, F.M., 2013. Rho signalling restriction by the RhoGAP Stard13 integrates growth and morphogenesis in the pancreas. Development 140:126—135.
[24] Hingorani, S., Petricoin, E., Maitra, A., Rajapakse, V., King, C., Jacobetz, M., et al., 2003. Preinvasive and invasive ductal pancreatic cancer and its early detection in the mouse. Cancer Cell 4:437—450.
[25] Herrera, P., 2000. Adult insulin- and glucagon-producing cells differentiate from two independent cell lineages. Development 127:2317—2322.
[26] Carter, J.D., Dula, S.B., Corbin, K.L., Wu, R., Nunemaker, C.S., 2009. A practical guide to rodent islet isolation and assessment. Biological Procedures Online 11:3—31.
[27] Tattikota, S., Rathjen, T., McAnulty, S., Wessels, H., Akerman, I., van de Bunt, M., et al., 2013. Argonaute2 mediates compensatory expansion of the pancreatic β cell. Cell Metabolism 19:122—134.
[28] Porat-Shliom, N., Milberg, O., Masedunskas, A., Weigert, R., 2013. Multiple roles for the actin cytoskeleton during regulated exocytosis. Cellular and Molecular Life Sciences 70:2099—2121.
[29] Geron, E., Boura-Halfon, S., Schejter, E., Shilo, B., 2015. The edges of pancreatic islet beta cells constitute adhesive and signaling microdomains. Cell Reports 10:317—325.
[30] Granot, Z., Swisa, A., Magenheim, J., Stolovich-Rain, M., Fujimoto, W., Manduchi, E., et al., 2009. LKB1 regulates pancreatic beta cell size, polarity, and function. Cell Metabolism 10:296—308.
[31] Wilson, J., Ludowyke, R., Biden, T., 2001. A redistribution of actin and myosin IIA accompanies Ca2-dependent insulin secretion. FEBS Letters 492:101—106.
[32] Kitamura, T., 2013. The role of FOXO1 in [beta]-cell failure and type 2 diabetes mellitus. Nature Reviews Endocrinology 9:615—623.

[33] Taylor, B.L., Liu, F.F., Sander, M., 2013. Nkx6.1 is essential for maintaining the functional state of pancreatic beta cells. Cell Reports 4:1262—1275.

[34] Gutierrez, G.D., Bender, A.S., Cirulli, V., Mastracci, T.L., Kelly, S.M., Tsirigos, A., et al., 2017. Pancreatic beta cell identity requires continual repression of non-beta cell programs. Journal of Clinical Investigation 127: 244—259.

[35] Cai, E.P., Casimir, M., Schroer, S.A., Luk, C.T., Shi, S.Y., Choi, D., et al., 2012. In vivo role of focal adhesion kinase in regulating pancreatic beta-cell mass and function through insulin signaling, actin dynamics, and granule trafficking. Diabetes 61:1708—1718.

[36] Rondas, D., Tomas, A., Soto-Ribeiro, M., Wehrle-Haller, B., Halban, P.A., 2012. Novel mechanistic link between focal adhesion remodeling and glucose-stimulated insulin secretion. Journal of Biological Chemistry 287:2423—2436.

[37] Yang, S.Y., Lee, J.J., Lee, J.H., Lee, K., Oh, S.H., Lim, Y.M., et al., 2016. Secretagogin affects insulin secretion in pancreatic beta-cells by regulating actin dynamics and focal adhesion. Biochemical Journal 473:1791—1803.

[38] Khalil, B.D., Hanna, S., Saykali, B.A., El-Sitt, S., Nasrallah, A., Marston, D., et al., 2014. The regulation of RhoA at focal adhesions by StarD13 is important for astrocytoma cell motility. Experimental Cell Research 321:109—122.

[39] Henquin, J., Nenquin, M., Stiernet, P., Ahren, B., 2006. In vivo and in vitro glucose-induced biphasic insulin secretion in the mouse. Diabetes 55:441—451.

[40] Fraccaroli, A., Franco, C.A., Rognoni, E., Neto, F., Rehberg, M., Aszodi, A., et al., 2012. Visualization of endothelial actin cytoskeleton in the mouse retina. PLoS One 7:e47488.

[41] Zhu, X., Hu, R., Brissova, M., Stein, R.W., Powers, A.C., Gu, G., et al., 2015. Microtubules negatively regulate insulin secretion in pancreatic beta cells. Developmental Cell 34:656—668.

[42] Nakamura, Y., Kaneto, H., Miyatsuka, T., Matsuoka, T., Matsuhisa, M., Node, K., et al., 2006. Marked increase of insulin gene transcription by suppression of the Rho/Rho-kinase pathway. Biochemical and Biophysical Research Communications 350:68—73.

